Nuclear Physics **A528** (1991) 225-241
North-Holland

THE BETA DECAY OF $^{18}C^{\star}$

M.S. PRAVIKOFF, F. HUBERT, R. DEL MORAL, J.-P. DUFOUR, A. FLEURY and D. JEAN

CEN Bordeaux-Gradignan/IN$_2$P$_3$, "Le Haut-Vigneau", F-33175 Gradignan Cedex, France

A.C. MUELLER

GANIL, B.P. 5027, F-14021 Caen Cedex, France[1]

K.-H. SCHMIDT and K. SÜMMERER

Gesellschaft für Schwerionenforschung mbH, Postfach 11 0552, D-6100 Darmstadt 11, Germany

E. HANELT

Institut für Kernphysik der Technischun Hochschule, D-6100 Darmstadt, Germany

J. FRÉHAUT, M. BEAU and G. GIRAUDET

CEA, Centre d'Etudes de Bruyères-le-Chatel, B.P.12, F-91680 Bruyères-le-Chatel, France

B.A. BROWN

National Superconducting Cyclotron Laboratory and Department of Physics, Michigan State University, East Lansing, Michigan 48824, USA

Received 1 November 1990

Abstract: ^{18}C has been produced as a projectile fragment in the interaction of a 60 MeV/u ^{22}Ne beam with a thick beryllium + carbon target. Using the LISE spectrometer of GANIL tuned according to the PFIS method allowed an unprecedented measurement of its β-delayed γ spectroscopy, along with redetermination of half-life and β-neutron branching ratio. A partial decay scheme is proposed. A comparison with theoretical predictions provides a qualitative understanding of the decay of ^{18}C.

E | RADIOACTIVITY ^{18}C; measured E_γ, I_γ, $T_{1/2}$, $\beta\gamma$-coin. ^{18}N deduced levels, β-branching. Compared with theory. Ge detector.

1. Introduction

Several experiments have already been carried out to study the nuclear properties of ^{18}C. Its mass has been measured, using charge exchange reactions [1,2]). An excited state of ^{18}N was observed in ref. [3]). Recent experiments performed at the GANIL facility have produced ^{18}C as a projectile-like fragment [4,5]), measuring its half-life and total β-neutron branching ratio P_n.

* Experiment performed at the GANIL National Accelerator, France

[1] Present address: Institut de Physique Nucléaire, B.P.1., F-91406 Orsay Cedex, France.

This paper presents the first β-delayed γ-spectroscopy of ^{18}C. Energies and relative intensities of γ-rays following the β-decay of ^{18}C have been measured. Several excited states in ^{18}N have been populated with charge exchange reactions [6]). Consequently a comparison can be made between our measured γ-rays and the experimental excitation energies of the daughter states. Since existing data on β-branchings to neutron unstable states of ^{18}N are given by liquid scintillator measurements [4,5]) with rather large systematic uncertainties, we feel it is important to have an independent P_n measurement.

Several shell-model calculations for ^{18}N have appeared previously in the literature [7-12]). Calculations based on the Millener–Kurath interaction [13]) are considered in this paper.

The first chapter describes the experimental setup, the data acquisition, the isotope identification method, along with the off-line data analysis procedures. The experimental results are given in sect. 2, while results are analysed and discussed in sect. 3. In sect. 4, we present the theoretical predictions of the ^{18}C β decay and their comparison with the experimental results.

2. The experiment

2.1. EXPERIMENTAL SETUP

This experiment was carried out with the LISE spectrometer [14]) at GANIL and deals with the formation of ^{18}C nuclei through the interaction of a 60 MeV/nucleon ^{22}Ne beam with a combined target of 286 mg · cm^{-2} Be and 60 mg · cm^{-2} C foils. A beam intensity of approximately 4×10^{11} s^{-1} was achieved for the runs concerned, totalizing more than 8 hours of beam, with almost 400,000 ^{18}C nuclei produced. The nuclei were separated by the LISE spectrometer, tuned according to the projectile fragments isotopic separation (PFIS) method [15,16]).

The schematic setup for the experiment is to be found in fig. 1. One Ge detector for γ-ray measurements, a silicon detector and plastic scintillators for β-measurements were part of the experimental apparatus. Through pulsed beam (300 ms on/300 ms off) and time measurements, half-lives were measured.

2.1.1. The spectrometer. The PFIS method requires a two-stage magnetic system, like the LISE spectrometer at GANIL, an apparatus consisting of two identical dipoles and ten quadrupoles. The target is located on a focal point in front of the first dipole, which is set to a $B\rho$ value (magnetic rigidity) allowing only projectile fragments with a specific A/Z ratio to be transmitted to the intermediate focal plane, half-way between the two dipoles. The first selection is made by adjustable slits limiting the $B\rho$ acceptance of the line.

At the intermediate focal plane, a thick shaped degrader (539 mg · cm^{-2} aluminium foil) is used to slow down the selected ions and to provide an extra separation of ions, based upon different momentum losses, depending on Z, A and energy of the

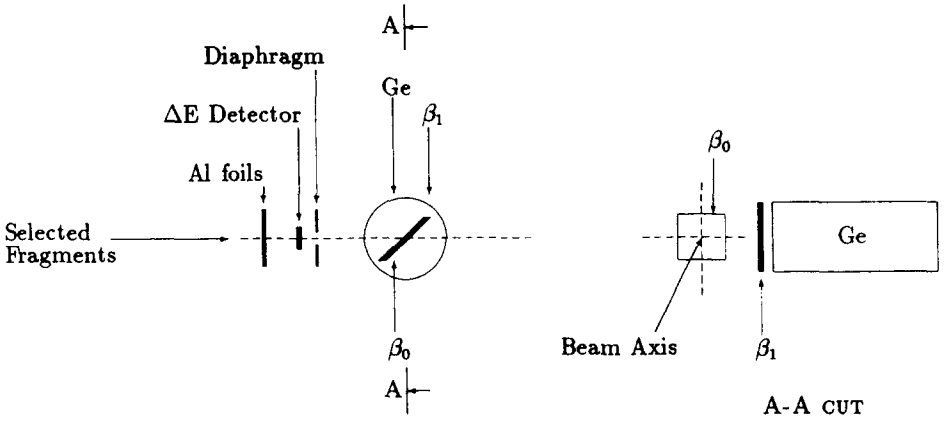

Fig. 1. The experimental setup is schematized in this figure, where the different elements are not drawn to scale. The ΔE detector is a silicon detector and β_0 and β_1 are plastic scintillators. Report to text for details.

fragment. This, in turn, makes it possible to tune the second dipole so that only those fragments with a specific momentum ratio p_2/p_1, corresponding to the value of $B\rho_2/B\rho_1$, are transmitted through this second stage, and fly directly to the measurement area at the exit focal plane.

The mathematical formalism of the PFIS method will not be discussed here since it has been reported in ref. [15]).

2.1.2. The detectors. The detection set-up has a two-fold purpose: (i) detect the implantation of the nuclei with a Si transmission detector and a scintillator used as a catcher, (ii) record the radioactivity of the selected isotope through β and γ counters. Detailed characteristics of these detectors are as follows:

(1) ΔE and time-of-flight: The ΔE detector is a 300μ silicon detector placed on the projectile fragments path, in front of all other detectors. This particular detector issues a ΔE and a time signal, which, combined to a radiofrequency (RF) signal coming from the GANIL accelerator, delivers a unique ΔE/time-of-flight identification of the isotopes passing-through.

(2) Plastic scintillators: A plastic scintillator has been placed along the beam axis. It is a rectangular flat piece of plastic with overall dimensions of 23 mm × 40 mm × 5 mm. As seen in fig. 1, it is mounted at an angle of 45° with respect to the beam. A light guide connects it to a photomultiplier. Aluminium energy degraders in front of the ΔE detector are adjusted in their thickness to stop the desired isotope in it. This scintillator acts then as a catcher to stop isotopes of interest, ensuring a high β-efficiency, and as a β-detector.

(3) Ge: The p-type Ge detector is a 174 cm^3 cylindrical crystal, with a specified resolution of 1.95 keV at 1.33 MeV and a peak-to-Compton ratio of 62:1. The standard efficiency is 40% with respect to a 3″ × 3″ NaI scintillator.

A thin plastic scintillator is positioned in front of the Ge detector. It can be used to increase the β-efficiency of the whole, but is more intended to eliminate unwanted β-counting in the germanium during the experiment as well as for the off-line analysis, where it acts as a veto detector.

2.2. DATA ACQUISITION AND CONTROL OF THE EXPERIMENT

All data was processed by the GANIL acquisition system, consisting of an array of CAMAC bins connected to a ModComp computer. Enhanced capabilities for on-line analysis and acquisition were achieved through the use of the CAmac Booster (CAB) module.

A "fast decision module" is at the heart of the GANIL acquisition system. It opens a time window of 600 ns duration for each relevant event, followed by a series of other time windows of various lengths, dedicated mainly to optional fast- and/or slow-coming rejection signals. These last windows amount, in this experiment, to an added blackout time of the acquisition of 5.77 μs between each event.

The dead-time of the acquisition was monitored for both on- and off-beam periods. This information is also stored for each event. Correction factors are 1.15 and 1.09, respectively.

For off-line analysis we recorded (i) the matrix of stroke detectors, (ii) a bitpattern unit for hard and software information (e.g. beam on/off, right type of ion yes/no, and so on.), (iii) quartz clock data on two different time scales, and (iv) quantitative information coming from the different detectors (i.e. mainly energy for the germanium detector). Concerning the germanium detector, dual electronics were set up to cover full-energy ranges of both round 5 and 10 MeV on 8k ADCs.

2.3. ISOTOPE IDENTIFICATION

With the LISE spectrometer tuned according to the PFIS mode, magnetic rigidities of the two dipoles were set to 3.012 T · m and 2.597 T · m, respectively. The momentum acceptance of the line was $\Delta p/p = \pm 2.5\%$.

Fig. 2 shows the transmission of ^{18}C and of the other isotopes, which we call contaminants. The numbers below each isotope identification indicate their abundance relative to ^{18}C, whose value is set to 1000.

The two-dimensional ΔE/TOF plot (fig. 3) shows the whole statistics accumulated during this experiment. Excellent separation of the isotopes is to be stressed, as well as the limited number of contaminants. The incident ^{22}Ne beam and the selected nucleus, ^{18}C, are isotones, and nuclear reaction mechanisms in this energy regime are known not to favor the production of nuclei with a number of neutrons larger than that of the beam. A total of 396, 073 ^{18}C nuclei were collected, out of 617, 724 nuclei transmitted during an 489 mn elapsed time. This amounts to an average of

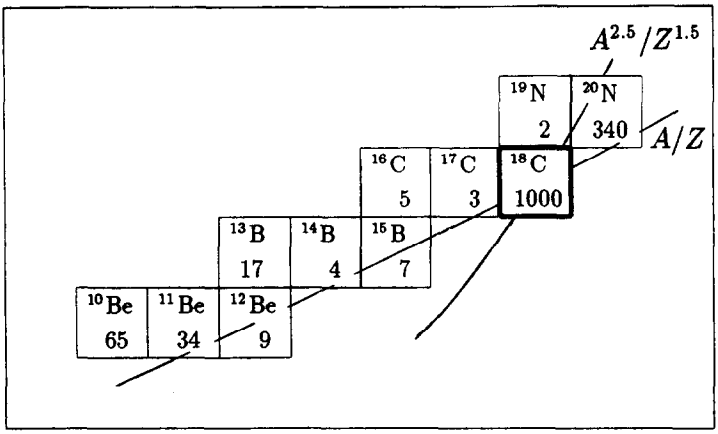

Fig. 2. This figure highlights the selection criteria (A/Z and $A^{2.5}/Z^{1.5}$) of the PFIS method. Only the transmitted nuclei are shown with their measured relative intensities, normalized to 1000 for ^{18}C.

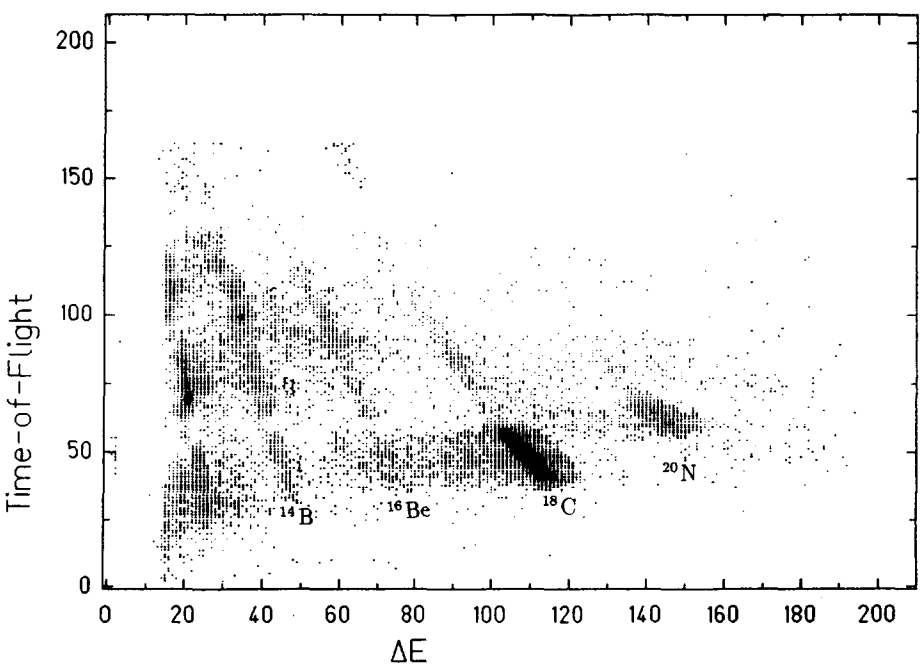

Fig. 3. Two-dimensional plot ΔE/time-of-flight showing experimental separation and identification of all nuclei selected by the PFIS method in this experiment.

13.5 ^{18}C nuclei per second. The prominent contaminant is ^{20}N, with a total number of only 32,937 nuclei, or 1.12 nucleus per second.

2.4. OFF-LINE DATA ANALYSIS

The off-line γ-ray analysis is highly automated via a computer program [17]), based upon a peak-search technique and fitting methods, adapted from those proposed by Phillips and Marlow [18]). Energy calibration, efficiency knowledge and pile-up corrections are carefully taken into account.

2.4.1. Energy calibration. Both external and internal energy calibrations of the γ-ray detectors have been made. For external calibration, a ^{152}Eu source has been counted in a near-to-experimental geometry. But since the ions studied are embedded in a plastic scintillator, concurrent off-line analysis of spectra of nuclides present with ^{18}C (notably ^{18}N and ^{19}O) is needed for the calculation of the energy calibration, using precisely-known γ-ray assignments. This calibration reveals that the final low-energy threshold, all components included from the detector to the computer, via the electronics, is around 40 keV.

2.4.2. Efficiency determination. The measurement of the photopeak efficiency and of the total efficiency as a function of γ-ray energy, along with the knowledge of the decay scheme, allows branching ratios to be determined. The photopeak efficiency curve was obtained by fitting the results of a measurement of the γ-rays of the $^{27}Al(p, \gamma)^{28}Si$ reaction. This experiment was made on the 4 MV Van de Graaff accelerator at the CEN Bordeaux Gradignan [17]).

A very important point for the subsequent analysis is the rapidly falling efficiency of germanium detectors for diminishing energies (mainly around 100 keV and less), which is a distinctive feature of such detectors. The ^{152}Eu source has low-energy rays, down to 39 keV, with known branching ratios. From the spectrum analysis of this isotope, we figured out a 24-fold drop in the efficiency curve from 122 to 39 keV. Absorption in the matter is also a critical parameter of the analysis. In particular, absorption in the plastic scintillator can generate uncertainties on the efficiency values, particularly at low γ-ray energies. Since up to 23 mm of plastic material has to be transversed by the γ-radiation before entering the germanium detector (fig. 1), according to tables of ref. [19]), an attenuation coefficient was calculated and incorporated to the mathematical formulation of the efficiency for γ-rays with energies lower than 300 keV.

Uncertainties of the order of 5% are to be expected for the photopeak efficiency, possibly reaching 30% for the low-energy domain, due to the lack of exact or near-to-exact experimental measurements for those very low energy points.

The total efficiency curve is obtained with ^{137}Cs and ^{60}Co radioactive sources, with uncertainties in the 10% range, raising for energies below 70 keV.

2.4.3. Pile-up corrections. Since we operate in a close-geometry configuration, summing corrections have to be made. They are of two types: random and

coincidence summing corrections. Random summing becomes important at high counting rates, while coincidence summing is due to gammas emitted in cascade within a time span shorter than the time resolution of the detector and/or the inherent time window of the analysis and recording hardware. These corrections have to be taken into account for both the determination of the detector efficiency, and, conversely, for the determination of branching ratios for experimental measurements.

Several authors have already pointed out the problem. A general treatment has been proposed by Andreev *et al.* [20]), but, as McCallum and Coote [21]) noted, their paper is not well known*. We started with the paper of Andreev. Two different programs were written, according to the system of equations proposed. The first one implies the knowledge of the decay scheme [excited levels, β-branching ratios, internal decay (γ-ray plus conversion) ratios], and of the photopeak and total efficiencies. It calculates the intensities of the γ-lines as they are expected to be observed in the experiment. The second one starts with experimental data, and, assuming a known level scheme, computes the γ- and β-branching ratios.

Both programs are purely analytical and have no limitation on the number of levels one can put into them**. It was checked that they are fully compatible with each other, and the first one was cross-checked with hand calculations on simple decay schemes.

3. The experimental results

3.1. GAMMA SPECTRA

Fig. 4 shows the full-range γ-spectrum obtained with the PFIS-selection criterion set for ^{18}C. Very low background is a main feature of the spectrum, along with a very clean identification of all lines. The prominent lines of the ^{18}C daughters (^{18}N and ^{17}N) are clearly seen in this spectrum. The most abundant nucleus apart from ^{18}C, namely ^{20}N, also produces some lines in the γ-spectrum.

Eleven γ-lines have been attributed to the β-decay of ^{18}C. Their energies and relative intensities are given in table 1, along with the associated uncertainties. The intensities have been normalized to the most intense γ-line (2614.2 keV). In table 1, the two lines marked with an asterisk (1374.8 and 1849.9 keV) had been previously observed in the β-decay of ^{17}C [ref. [22])]. But, due to the very low counting rate of ^{17}C (0.1% of ^{18}C) measured in the two-dimensional plot (ΔE/TOF), the observation of the γ-lines following the β-decay of ^{17}C is not expected. Those two lines indicated

* A misprint is to be found in the formula (13) of the paper of Andreev *et al.*, which should read: $\chi_{ik} = K_{ik}(1+\alpha_{ik})/(\varepsilon_{ik}^{b} N_i)$. Also in the paper of McCallum and Coote, formula (7) was misprinted and should be: $M_k = \sum_{j=0}^{k-1} b_{kj} M_j$.

** These programs are written in REXX language, to be run on VM- and MVS-based IBM mainframes, but can be easily adapted to any high-level language. They are available from the authors upon request (E-mail: PRAVIKOF@FRCPN11).

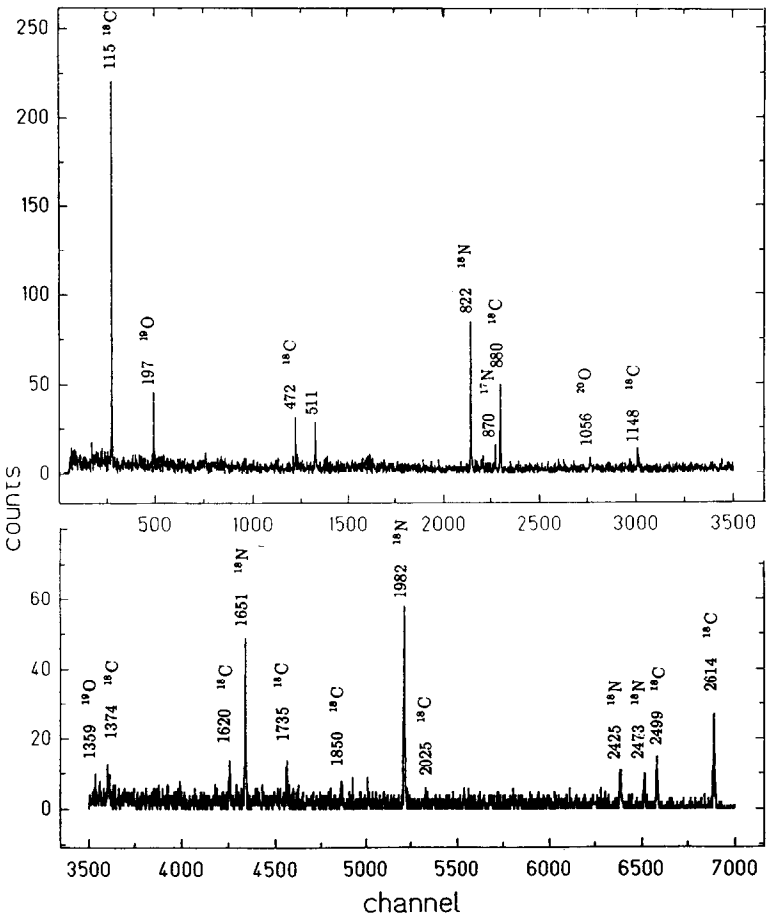

Fig. 4. γ-ray spectrum measured in coincidence with the β decay of ^{18}C nuclei.

TABLE 1

Measured energies and relative intensities of γ-rays assigned to the β^- decay of ^{18}C

E_γ	I_γ	E_γ	I_γ
114.9 (2)	32 (1)	1734.8 (4)	25 (5)
471.7 (2)	15 (2)	1849.9 (4)*	11 (5)
879.7 (2)	44 (4)	2025.3 (8)	7 (5)
1147.8 (4)	17 (5)	2499.3 (4)	41 (9)
1374.0 (10)*	24 (5)	2614.2 (4)	100 (11)
1619.9 (3)	25 (5)		

Numbers in parentheses following any value represent the uncertainty on the last digit(s). The two lines indicated with an asterisk are associated to the β-delayed neutron emission. The intensities have been normalized to 100 for the 2614 keV line.

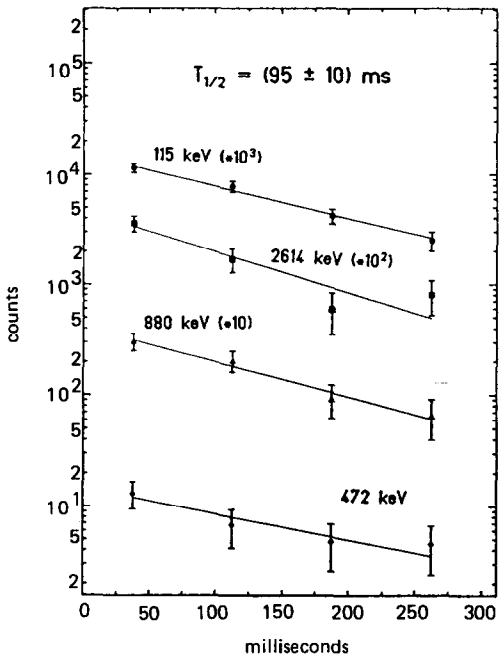

Fig. 5. Off-beam multispectrum analysis of the half-life of ^{18}C. The data points represent the intensities of the four most intense lines of ^{18}C, recorded in four subsequent time intervals. The lines correspond to individual fits. The weighted average of these fits gives $T_{1/2} = 95 \pm 10$ ms for the half-life of ^{18}C.

with an asterisk are associated to the transition to the ground state of the two known first levels in ^{17}N (1373.9 and 1849.6 keV), populated by the β-delayed neutron emission of ^{18}C.

3.2. HALF-LIFE OF ^{18}C

Fig. 5 presents the decay during a 300 ms beam-off period of the four most intense γ-rays associated with the ^{18}C decay. Due to low statistics, the decay curves for the other lines have not been presented. Independent determinations of all lines agree

TABLE 2

Theoretical and experimental $T_{1/2}$ and P_n values for ^{18}C

$T_{1/2}$ (ms)	P_n(%)	Refs.	Comments
95 ± 10	19 ± 5		this work
66^{+25}_{-15}	25 ± 4.5	[4]	experiment
78^{+20}_{-15}	50 ± 10	[5]	experiment
130–136	51	[23]	Gross theory of β-decay
64		[24]	improved Gross theory
124		[25]	microscopic model
89		[26]	second-generation microscopic calculations

with the compound value $T_{1/2} = 95 \pm 10$ ms. The half-life obtained in this work is compared in table 2 to experimental values published recently. Note that the present measurement, though within the error bars consistent with the two recently published half-life values, is more precise.

We have also listed in table 2 the different theoretical half-life predictions which are available [23-26]). Obviously, no significant difference is to be noted between our value and the various predictions.

4. Analysis

First, the total β-decay probabilities of ^{18}C to the ground state and the γ-emitting states of ^{18}N (P_γ) was deduced from a comparison of two simultaneous experiments as discussed below. Second, from the observed γ-ray energies and intensities, we propose a decay scheme of ^{18}C to γ-emitting states in ^{18}N.

4.1. DETERMINATION OF THE $^{18}C(\beta^-)^{18}N$ TOTAL BRANCHING RATIO

One of the characteristics of the PFIS method used in this experiment is that the daughters following the (β, γ) and (β, n) decays of the selected nuclei are never directly transmitted by the spectrometer, as evidenced in fig. 3. It follows that ^{18}N and ^{17}N nuclei are observed as daughters only in the γ spectrum. In turn, this means that the measurement of their activity, integrated over beam-on and beam-off cycles, gives in principle access to the $^{18}C(\beta^-)^{18}N$ and $^{18}C(\beta^-n)^{17}N$ decay probabilities. Unfortunately, the ^{18}N and ^{17}N β-decays are not sufficiently known to be a real support for such measurements: (i) the branching ratios for ^{18}N decay to γ-emitting states reported by Olness *et al.* [7]) requires normalization, as shown by Zhao *et al.* [9]) and, up to now, no measurement is available; (ii) the $^{18}N(\beta^-n)^{17}O$ decay would imply the feeding of excited states in ^{17}O, which cannot be discriminated from the $^{17}N(\beta^-)^{17}O$ decay.

To settle this problem, the following procedure has been developed. The LISE spectrometer has been tuned to transmit ^{18}N only, all other experimental conditions remaining unchanged. Therefore we can assume the same transmission factor for both, ^{18}C and ^{18}N. The total number S^N of ^{18}N ions impinging on the ΔE detector has been compared to the activity A^N of its prominent 1982 keV γ-line, detected by the Ge detector. The ratio (A^N/S^N) gives a link factor which differs from the real one by the unknown γ branching ratio of the 1982 keV line. Going back to the ^{18}C experiment, the ratio (A^C/S^C), where A^C is the activity of the 1982 keV γ-line (deduced from fig. 4) and S^C the number of ^{18}C nuclei impinging on the ΔE detector (fig. 3), deviates from the above ratio (A^N/S^N) by the ^{18}C β-decay probability, P_γ, to γ-emitting states plus to the ground state of ^{18}N.

$$P_\gamma = \frac{A^C/S^C}{A^N/S^N} = (81 \pm 5)\% .$$

Because several ^{18}N γ-lines were used to calculate P_γ, the P_γ value above represents the mean value with its standard error.

The β-decay of ^{18}C to alpha-particle emitting states in ^{18}N is energetically not possible. Then the β-delayed neutron emission, P_n, is directly deduced from P_γ as follows:

$$P_n = 1 - P_\gamma = (19 \pm 5)\%$$

Recently, two quite different values have been reported for the β-delayed neutron emission probability of ^{18}C: (25 ± 4.5)% [ref. [4])] and (50 ± 10)% [ref. [5])]. Our value matches best that of ref. [4]), although we have to keep in mind that there are inherent systematic uncertainties on the efficiency calibration of the liquid scintillator for the quoted references.

4.2. BETA DECAY OF ^{18}C TO GAMMA EMITTING STATES

States in ^{18}N have previously been populated by charge exchange reactions [3,6]). Essentially two levels at 121 (10) and 747 (10) keV have been found. Additional excited states were observed at 0.575, 2.21 and 2.42 MeV. These levels are shown on the right-hand side of fig. 6.

Since no coincidence data have been obtained in the present work, the assignment of γ-ray peaks to ^{18}N transitions was made on the basis of intensity and energy considerations only. Table 3 gives the proposed identification of the transitions. Two γ-rays (115 and 472 keV) can be fitted into the lowest experimental levels of ^{18}N. Two levels are established at 1735 and 2614 keV. Their existence is rather certain since both crossover and cascade transitions can be assigned. The excited states deduced from the ^{18}N transition energies obtained in this work are shown on the left-hand side of fig. 6. However, by considering the experimental intensities given in table 1, it appears clearly that the I_γ value of the 115 keV line is much lower (more than a factor 2) than what is to be expected from the proposed assignments in table 3. From the present data alone, one cannot completely exclude a different decay scheme. But obviously the nice fit of the observed γ-rays within the proposed four levels strongly favors such a decay scheme.

One reason for the low intensity measured for the 115 keV line could originate in a delayed transition between low lying levels of ^{18}N, not detected in the present work due to experimental limitations. Such a delayed transition has been observed in the neighboring nucleus ^{16}N between its first excited state ($E_x = 120$ keV, $J^\pi = 0^-$) and its ground state ($J^\pi = 2^-$). In the case of ^{18}N, shell-model calculations predict a low-lying multiplet of states (within 150 keV of the ground state) with spin values $J^\pi = 1^-, 2^-, 3^-$ [refs. [6,7,10])]. Clearly ^{16}N and ^{18}N have similarities and the existence of a low-lying level in ^{18}N with a mean lifetime in the μs range is possible. From the experimental point of view, it must be remembered that only the γ events in coincidence with β decays within a 600 ns coincidence window have been recorded

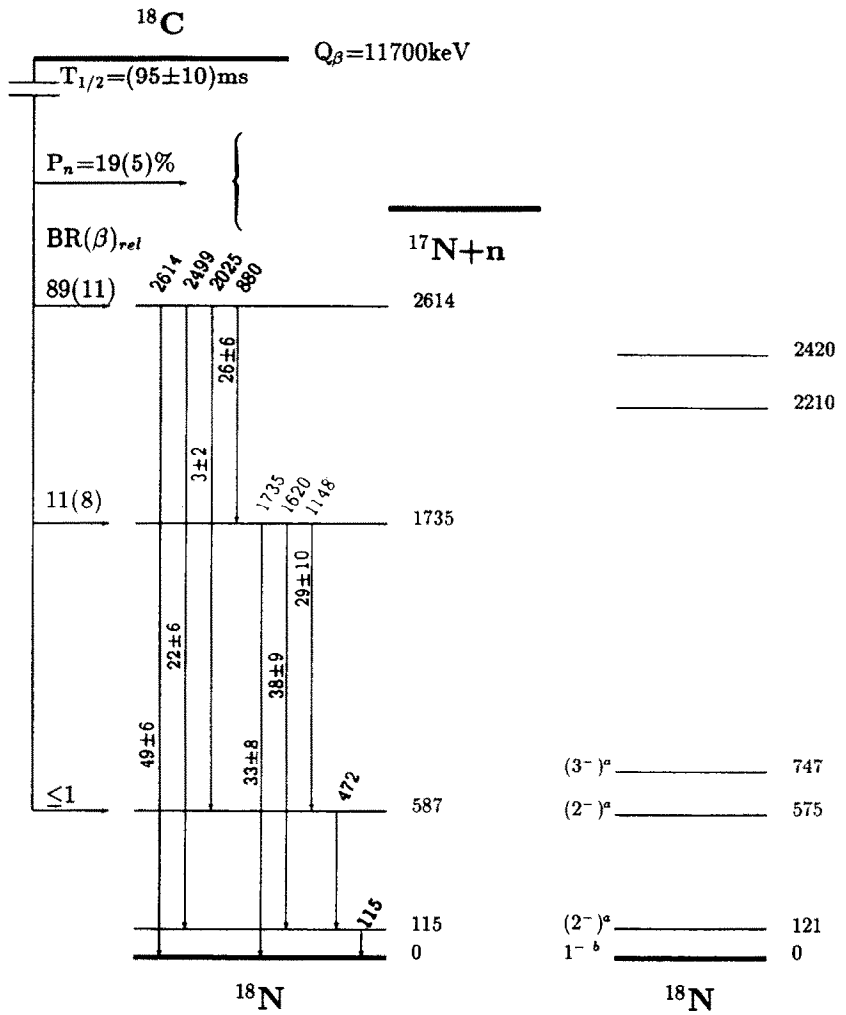

Fig. 6. Partial decay scheme of ^{18}C illustrating β- and γ-ray branches observed in the present experiment (left-hand side). The quoted ^{18}C β-branching ratios to γ-emitting states have been normalized to 100. For absolute β branchings, report to table 4. The energies of the observed transitions are indicated in keV above the transition arrows. The corresponding intensities located on the side of the arrows are such that the total flux out of a level is 100. On the right-hand side the experimental levels previously observed in a charge exchange reaction are presented. The spin-parity values labelled with *a* are suggested in ref. [10]); those labelled with *b* are from ref. [7]).

in the present experiment. The consequence is that if a γ-transition is delayed, all events emitted after this 600 ns window are lost. Moreover, in the low-energy region ($E_\gamma \leq 100$ keV) the efficiency of the Ge detector decreases steeply due to the absorption in the plastic detector where the ^{18}C nuclei are implanted (the electronic threshold being around 40 keV). Any transition with an energy below this threshold cannot be observed in this experiment.

TABLE 3

Assignment of γ-rays observed in ^{18}C $(\beta^-)^{18}N$

^{18}N Transitions (keV)			BR (in %)
E_γ	E_i	E_f	
114.9 (2)	115	0	100
472.7 (2)	587	115	100 (16)
1734.8 (4)	1735	0	33 (8)
1619.9 (3)	1735	115	38 (9)
1147.8 (4)	1735	587	29 (10)
2614.2 (4)	2614	0	49 (8)
2499.3 (4)	2614	115	22 (6)
2025.3 (8)	2614	587	3 (2)
879.7 (2)	2614	1735	26 (6)

The branching ratios (BR) are normalized to get 100% flux out of a level, taking into account corrections for summing effects. Numbers in parentheses following any given value represent the uncertainty on the last digits. E_i and E_f are the initial and final level energies, respectively, with $E_\gamma = E_i - E_f$.

It then appears that the existence of a low-energy level with a mean lifetime much larger than what is usually measured for γ-emitting states would explain that only part of the flux out of the 115 keV level is detected. In the following we have adopted such an hypothesis to calculate γ- and β- branching ratios from the proposed assignments of the γ-rays. The intensity values of table 1 have been used except, obviously, the I_γ value of the 115 keV which has been adjusted such that the γ-flux feeding the 115 keV level is equal to the flux depopulating this level. The calculated branching ratios take into account the effect of coincidence summation of γ-radiations. In the present case where a close geometry is used and where the proposed decay scheme results in many possible combinations of summing of two or more coincident γ-rays, large coincidence summing effects are observed. They have been calculated with the recursive formulas of refs. [20,21]). The given branching ratios take into account the uncertainty in the efficiency curve of the Ge detector and the statistical uncertainties.

In table 3 the calculated γ-branching ratios (BR) are given. It must be noticed that the BR values presented do not depend on the intensity value of the 115 keV line, since in the proposed decay scheme, this line feeds the ground state only.

The calculated β^- branching ratios are presented in table 4. As already mentioned, the experimental value P_γ includes the β-decay to the ^{18}N ground state and γ-emitting states. The ground-state spin and the parity of ^{18}N have been determined experimentally to be 1^- [ref. [7])]. A first forbidden branch to the ground state of ^{18}N is not expected to be large within the error bars and thus we can reasonably well estimate that the measured value of $P_\gamma = 0.81 \pm 0.05$ represents the β decay to γ-emitting states only.

TABLE 4

^{18}C β-ray branching ratios and log *ft* values

E_x (keV)	BR(β^-) (%)	log *ft*
115		
587	≤1	≥6.36
1735	9 (7)	5.18 (78)
2614	72 (10)	4.11 (22)

The branching-ratio values in table 4 have been calculated with the hypothesis that there is no direct β-feeding of the 115 keV level. Once again, the calculated spin and parity values for the low-lying levels in ^{18}N ($2^-, 3^-$), support this hypothesis [6,7,10]).

For β-feeding of the 587 and 1735 keV levels, one must notice that the calculated values are rather unsensitive even to a large change in the intensity of the 115 keV γ-line. One observes almost no direct β-feeding to the 587 keV level (≤1%). The β decay to the 1735 keV level is (9±7)% only. Most of the β-feeding is then concentrated on the 2614 keV level. The decay scheme of ^{18}C deduced from the present experiment is shown on the left side of fig. 6.

The log *ft* values are presented in table 4. They have been calculated using $T_{1/2} = 95$ ms (as determined in the present work), $Q_\beta = 11.770$ MeV [ref. [27])] and the present level energies and intensities, using the tabulations of Gove and Martin [28]).

The accepted criteria for the spin and parity assignments from log *ft* values include the empirical rule: for $Z < 80$, if log *ft* < 5.9, the transition is allowed and $\Delta I = 0$ or 1, $\Delta\pi = +$, no $0 \rightarrow 0$ transitions [29]). In β-decay of ^{18}C then, the decay to the 2614 keV level (with log *ft* = 4.11) is allowed and the 2614 keV state in ^{18}N is $J^\pi = 1^+$. The β-decay to the 1735 keV level is not quite strong enough to allow an unambiguous assignment by the criterion given above and thus it could have $J = 1, 2$.

According to the mass of ^{18}N ground state and the systematics for Coulomb energies, its isobaric state in ^{18}O should have an excitation energy of 16.214 MeV [ref. [30])]. For ^{18}O, several experimental investigations have been performed in the excitation energy region of interest here, above 16 MeV. A complete compilation is to be found in ref. [31]). Two strongly excited levels in ^{18}O have been identified with J^π; $T = 2^-$; 2 and J^π; $T = 1^+$; 2 at 16.399 MeV and 18.871 MeV, respectively, in a high-resolution $^{18}O(e, e')$ experiment [11]). The close connection of these last states and the 115 keV and 2614 keV levels in ^{18}N deduced from this work supports evidence that they are analogue states. Several other weak states have also been observed in this (e, e') experiment, but no definite *J* and *T* assignments have been made. The comparison between our experimental results and the levels in ^{18}O shows that there are experimental candidates for the analogue of the 587 keV and 1.735 MeV levels in ^{18}O.

5. Theoretical predictions

As already mentioned, several groups have published shell-model calculations for ^{18}N [refs. [7-12])]. For the low-lying negative-parity states the assumed model space is one proton hole in the 0p shell coupled to three neutron particles in the 0s1d shell. An important ingredient in these calculations is the particle-hole interaction. Most previous calculations [7-9,11,12]) are based on the Millener-Kurath (MK) interaction [13]). It is known, however, that this MK interaction predicts a 2^- ground state for ^{18}N in contradiction to the assignment of 1^- from β decay [7]). Barker [10]) has noted that this discrepancy is related to the fact that the MK interaction inverts the order of the close-lying $2^-, 3^-$ doublet arising from the dominant $p_{1/2}^{-1} \times d_{5/2}^{1}$ configuration relative to the experiment. In the extreme weak-coupling picture low-lying 2^- and 3^- states in ^{18}N arise from the $p_{1/2}^{-1} \times (sd)^3 (J = \frac{5}{2}^+)$ configuration and low-lying 1^- and 2^- states arise from the $p_{1/2}^{-1} \times (sd)^3 (J = \frac{3}{2}^+)$ configuration. Thus, another important consideration for the precise ordering of the low-lying $1^-, 2^-, 2^-, 3^-$ multiplet in ^{18}N is the spacing of the $\frac{3}{2}^+, \frac{5}{2}^+$ doublet in ^{19}O. Barker showed that an interaction which is modified to reproduce the ^{16}N and ^{19}O spectra, also correctly predicts a 1^- spin for the ^{18}N ground state. This modified interaction gives a low-lying quartet of levels in qualitative agreement with the energies and J^π assignments shown on the right-hand side of fig. 6.

The ^{18}C decay has been calculated with the MK interaction in conjunction with similar calculations for other nuclei in this region [32]). The calculated level energies and branching ratios are given in table 5. It is difficult with these calculations to predict the energy gap between the lowest negative and positive-parity states to better than about one MeV, and for the purpose of calculating the half-life and branching ratios we have previously chosen to line up the energy of the lowest calculated positive-parity state with the lowest one known experimentally. In this case we give the results in table 5 for two choices of this excitation energy. In the first case, we assume that the lowest 1^+ state is the one observed experimentally at 2.614 MeV. In this case the calculated half-life is 197 ms, which is a factor of two larger than the experimental value, and the branching is dominated by decays to higher 1^+ states which are neutron unbound in disagreement with the experiment.

TABLE 5

Calculated *ft* values and branching ratios to low-lying 1^+ states in ^{18}N based on two different assumptions for the energy of the lowest 1^+ state

log *ft*	E_x (MeV)	BR (%)	E_x (MeV)	BR (%)
4.86	2.614	30.4	1.735	27.5
5.68	3.555	2.8	2.676	2.7
4.43	4.124	35.6	3.245	34.7
4.39	5.189	20.4	4.310	21.2
	>6.000	10.8	>5.200	13.9

In the second case, we assume that the state weakly populated in the experiment at 1.735 MeV is the lowest 1^+ state. In this case the calculated half-life is 117 ms in good agreement with experiment. Also the *ft* values are in rough agreement with experiment if we associate the 1^+ state predicted to be at 3.245 MeV with the strong one observed at 2.614 MeV. In either case we predict too much decay to neutron-unbound states. This discrepancy seen here must be closely connected with a similar problem for the decay of ^{16}C to ^{16}N, where MK calculations predict much too little strength to the lowest 1^+ state [33]). We have also made calculations for the ^{16}C and ^{18}C decays with the modified MK interaction discussed above. However, the difficulties encountered in reproducing the experimental features of the β-decay of ^{18}C persist. The modification to the MK interaction discussed above only concerns the $T=1$ component of the particle-hole interaction, whereas the structure of the 1^+ states in ^{16}N and ^{18}N will also depend on the $T=0$ component.

The final question we address is the isomeric nature of the 115 MeV level and the decay pattern within the low-lying states. In this discussion 1^-, 2^- and 2^- assignments for the ground state and the states at 115 keV and 587 keV are assumed, respectively. The transitions are then dominated by M1 decay. For comparison we can take the known value of $B(\mathrm{M1}) = (0.030 \pm 0.002)\mu_n^2$ for the $\frac{3}{2}^+$ to $\frac{5}{2}^+$ transition in the neighboring nucleus ^{19}O [ref. [34])]. If the 2^- to 1^- 115 keV transition had the same $B(\mathrm{M1})$ value, its lifetime would be 1.2 ns, much too short to account for the apparent isomeric nature (>600 ns) observed for this level. We have calculated the $B(\mathrm{M1})$ values with both the original MK interaction and the modified MK interaction and find extremely different results. We conclude that the 115 keV transition might be understood as an unusually hindered M1 transition, however, we believe that the present set of interactions is not good enough to make final conclusions about these transition rates.

6. Conclusion

This paper reports on the first βγ spectroscopic study of ^{18}C. Eleven γ-lines have been attributed to its β-decay. Values for the excitation energy of ^{18}N levels have been deduced. The two lowest ones are consistent with previously published values. Two levels, hitherto unobserved, are established at 1735 and 2614 keV. From the present experiment, a partial decay scheme of ^{18}C has been obtained.

Concerning the shell-model description of the β decay of ^{18}C, we conclude that the Millener–Kurath interaction, as modified by Barker, is adequate for a qualitative understanding of the decay of ^{18}C and the structure of ^{18}N. However, taking into account the problems which continue to exist, we feel that improved effective inteactions are highly needed in this mass region, which is important for testing shell-model calculations. The "interim step" started in ref. [32]) should be completed.

References

1) K.K. Seth, H. Nann, S. Iversen, M. Kaletka, J. Hird and H.A. Thiessen, Phys. Rev. Lett. **41** (1978) 1589
2) L.K. Fifield, J.L. Durell, M.A.C. Hotchkis, J.R. Leigh, T.R. Ophel and D.C. Weisser, Nucl. Phys. **A385** (1982) 505
3) F. Naulin, C. Détraz, M. Roy-Stephan, M. Bernas, J. de Boer, D. Guillemaud, M. Langevin, F. Pougheon and P. Roussel, Phys. Rev. **C25** (1982) 1074
4) A.C. Mueller, D. Bazin, W.C. Schmidt-Ott, R. Anne, D. Guerreau, D. Guillemaud-Mueller and M.-G. Saint-Laurent, Z. Phys. **A330** (1988) 63
5) M. Lewitowicz, Yu.E. Penionzhkevich, A.G. Artukh, A.M. Kalinin, V.V. Kamanin, S.M. Lukyanov, Nguyen Hoai Chau, A.C. Mueller, D. Guillemaud-Mueller, R. Anne, D. Bazin, C. Détraz, D. Guerreau, M.-G. Saint-Laurent, V. Borrel, J.-C. Jacmart, F. Pougheon, A. Richard and W.D. Schmidt-Ott, Nucl. Phys. **A496** (1989) 477
6) G.D. Putt, L.K. Fifield, M.A.C. Hotchkis, T.R. Ophel and D.C. Weisser, Nucl. Phys. **A399** (1983) 190
7) J.W. Olness, E.K. Warburton, D.E. Alburger, C.J. Lister and D.J. Millener, Nucl. Phys. **A373** (1982) 13
8) E.K. Warburton and D.J. Millener Phys. Rev. **C39** (1989) 1120
9) Z. Zhao, M. Gai, B.J. Lund, S.L. Rugari, D. Mikolas, B.A. Brown, J.A. Nolen, Jr., M. Samuel, R.I. Verral, J.C. Hardy and R.E. Bell, Phys. Rev. **C39** (1989) 1985
10) F.C. Barker, Austral. J. Phys. **37** (1984) 17
11) D. Bender, A. Richter, E. Spamer, E.J. Ansaldo, C. Rangacharyulu and W. Knüpfer, Nucl. Phys. **A406** (1983) 504
12) N.A. Orr, W.N. Catford, L.K. Fifield, M.A.C. Hotchkis, T.R. Ophel, D.C. Weisser and C.L. Woods, Nucl. Phys. **A491** (1989) 443
13) D.J. Millener and D. Kurath, Nucl. Phys. **A255** (1975) 315
14) R. Anne, D. Bazin, A.C. Mueller, J.-C. Jacmart and M. Langevin, Nucl. Instr. Meth. **A257** (1987) 215
15) J.-P. Dufour, R. Del Moral, H. Emmermann, F. Hubert, D. Jean, C. Poinot, M.S. Pravikoff, A. Fleury, H. Delagrange and K.-H. Schmidt, Nucl. Instr. Meth. **A248** (1986) 267
16) F. Hubet, J.-P. Dufour, R. Del Moral, H. Emmermann, D. Jean, C. Poinot, M.S. Pravikoff, A. Fleury, H. Delagrange, H. Geissel and K.-H. Schmidt, J. de Phys. **47** (1986) C4-229
17) D. Jean, Thèse d'Université, Bordeaux I, France, CENBG 8717 (1987)
18) G.W. Phillips and K.W. Marlow, Nucl. Instr. Meth. **137** (1976) 525
19) E. Storm and H.I. Israel, Nucl. Data Tables **7** (1970) 565
20) D.S. Andreev, K.I. Erokhina, V.S. Zvonov and I.Kh. Lemberg, Physicotechnical Institut Leningrad, UDC 539.108, 1358 (1972); translated from Prib. Tekh. Eksp. **No. 5** (1972) 63
21) G.J. McCallum and G.E. Coote, Nucl. Instr. Meth. **130** (1975) 189
22) J.-P. Dufour, R. Del Moral, A. Fleury, F. Hubert, D. Jean, M.S. Pravikoff, H. Delagrange, H. Geissel and K.-H. Schmidt, Z. Phys. **A324** (1986) 487
23) K. Takahashi, Prog. Theo. Phys. **47** (1972) 1500
24) T. Tachibana, S. Ohsugi and M. Yamada, Proc. 5th Int. Conf. on nuclei far from stability, Rosseau Lake, Ontario, Canada, Sep. 14-19, 1987, ed. I.S. Towner (AIP Conf. proc. 164) p. 614
25) H.V. Klapdor, J. Metzinger and T. Oda, At. Data Nucl. Data Tables **31** (1984) 81
26) A. Staudt, E. Bender, K. Muto and H.V. Klapdor-Kleingrothaus, At. Data Nucl. Data Tables **44** (1990) 79
27) A.H. Wapstra and G. Audi, Nucl. Phys. **A432** (1985) 1
28) N.B. Gove and M.J. Martin, At. Data Nucl. Data Tables **10** (1971) 205
29) S. Raman and N.B. Gove, Phys. Rev. **C7** (1973) 1995
30) M.S. Antony, J. Britz and A. Pape, At. Data Nucl. Data Tables **34** (1986) 279
31) F. Ajzenberg-Selove, Nucl. Phys. **A475** (1987) 1
32) M.S. Curtin, L.H. Harwood, J.A. Nolen, B. Sherrill, Z.Q. Zie and B.A. Brown, Phys. Rev. Lett. **56** (1986) 34; M. Samuel, B.A. Brown, D. Mikolas, J. Nolen, B. Sherrill, J. Stevenson, J.S. Winfield and Z.Q. Xie, Phys. Rev. **C37** (1988) 1314
33) D.E. Alburger and D.H. Wilkinson, Phys. Rev. **C13** (1976) 835;
K.A. Snover, E.G. Adelberge, P.G. Ikossi and B.A. Brown, Phys. Rev. **C27** (1983) 1837
34) P.M. Endt, At. Data Nucl. Data Tables **23** (1979) 3